The geometry of decision-making

Vivek Hari Sridhar[a,b,c,1], Liang Li[a,b,c,1], Dan Gorbonos[a,b,c], Máté Nagy[a,b,c,d,e,f], Bianca R. Schell[g], Timothy Sorochkin[h,i], Nir S. Gov[i] and Iain D. Couzin[a,b,c,1]

[a]Department of Collective Behaviour, Max Planck Institute of Animal Behavior, Konstanz, 78464 Konstanz, Germany

[b]Centre for the Advanced Study of Collective Behaviour, University of Konstanz, 78464 Konstanz, Germany

[c]Department of Biology, University of Konstanz, 78464 Konstanz, Germany

[d]MTA-ELTE Statistical and Biological Physics Research Group, Hungarian Academy of Sciences, 1117, Budapest, Hungary

[e]MTA-ELTE 'Lendület' Collective Behaviour Research Group, Hungarian Academy of Sciences, 1117, Budapest, Hungary

[f]Department of Biological Physics, Eötvös Loránd University, 1117, Budapest, Hungary

[g]Department of Chemistry, University of Konstanz, 78464 Konstanz, Germany

[h]Department of Physics & Astronomy, University of Waterloo, Waterloo, ON N2L 3G1, Canada

[i]Department of Chemical and Biological Physics, Weizmann Institute of Science, Rehovot 76100, Israel

Choosing among spatially-distributed options is a central challenge for animals, from deciding among alternative potential food sources or refuges, to choosing with whom to associate. Using an integrated theoretical and experimental approach (employing immersive virtual reality), we consider the interplay between movement and vectorial integration during decision-making regarding two, or more, options in space. In computational models of this process we reveal the occurrence of spontaneous and abrupt "critical" transitions (associated with specific geometrical relationships) whereby organisms spontaneously switch from averaging vectorial information among, to suddenly excluding one, among the remaining options. This bifurcation process repeats until only one option---the one ultimately selected---remains. Thus we predict that the

brain repeatedly breaks multi-choice decisions into a series of binary decisions in space-time. Experiments with fruit flies, desert locusts, and larval zebrafish reveal that they exhibit these same bifurcations, demonstrating that across taxa and ecological context, we show that there exist fundamental geometric principles that are essential to explain how, and why, animals move the way they do.

Animals constantly face the need to make decisions, and many such decisions require choosing among multiple spatially-distributed options. Despite this, most studies have focused on the outcome of decisions (1–3) (i.e. which option among alternatives is chosen), as well as the time taken to make decisions (4–6), but seldom on the movement of animals throughout the decision-making process. Motion is, however, crucial in terms of how space is represented by organisms during spatial decision-making; the brains of a wide range of species, from insects (7, 8) to vertebrates (9, 10), have been shown to represent egocentric spatial relationships, such as the position of desired targets, via explicit vectorial representation (11, 12). Such neuronal representations must, and do, change as animals move through space. Thus, while the movement of an animal may, initially, appear to simply be a readout of the decision made by the brain—and consequently not particularly informative—this view overlooks important dynamical properties introduced into the decision-making process that result from the inevitable time-varying geometrical relationships between an organism and spatially-distributed options (i.e. potential 'targets' in space).

Due to a dearth of existing studies, and with the objective to develop the necessary foundational understanding of the 'geometry' of decision-making, we focus here—first theoretically and then experimentally—on the consequences of the recursive interplay between movement and (collective) vectorial integration in the brain during relatively simple spatial decisions. We

52 employ immersive virtual reality to investigate decision-making regarding multiple (2 or more)
53 options in both invertebrate (the fruit fly *Drosophila melanogaster*, and desert locust
54 *Schistocerca gregaria*) and vertebrate (larval zebrafish *Danio rerio*) models. Doing so allows
55 us to reveal the emergence of geometric principles that transcend the study organism and the
56 decision-making context, and thus are expected to be broadly relevant across taxa. In support
57 of this finding we also explore how these principles extend to collective decision-making in
58 mobile animal groups, allowing us to gain insights across three scales of biological
59 organisation, from neural dynamics, to both individual and collective decision-making.
60

61 ## Modelling decision-making on the move

62 Congruent with neurobiological studies of the invertebrate and vertebrate brain, we consider
63 organisms to have an egocentric vectorial representation of spatial options (11–13). We then
64 consider the collective dynamics of vector integration in the brain assuming there exists
65 reinforcement (excitation/positive feedback) among neural ensembles that have similar
66 directional representations (goal vectors), and global inhibition and/or negative feedback (both
67 produce broadly similar results, see SI Appendix and Fig. S1) among neural ensembles that
68 differ in vectorial representation. This captures, in a simple mathematical formulation, the
69 essence of both explicit ring-attractor networks (as found in insects (7)), and computation
70 among competing neural groups (as in the mammalian brain (14)). The animal's relative
71 preference for a target is given by activity of neurons that encode direction to that target relative
72 to activity of neurons that encode direction to other targets, and the angular sensitivity of the
73 neural representations (angular difference at which excitation no longer occurs) is specified by
74 a neural tuning parameter, ν. The network then computes, spontaneously via iterative collective
75 dynamics, a unique 'consensus' vector ('activity bump') that, along with some angular noise,
76 represents the animal's desired direction of movement (Fig. S2). This is then translated into

77 motor output (see SI Appendix for model details (15)). Stochasticity in neural dynamics is
78 implemented here as the neural noise parameter, T.
79
80 While capturing known, generic features of neural integration, our model is deliberately
81 minimal. This serves multiple purposes: firstly, following principles of maximum parsimony
82 we seek to find a simple model that can both predict and explain, the observed phenomena;
83 secondly, we aim to reveal general principles and thus consider features that are known to be
84 valid across organisms irrespective of inevitable difference in structural organization of the
85 brain; thirdly, analytical tractability of our model provides deeper insights into the system
86 dynamics; and, finally, our results are shown to be extremely robust to model assumptions,
87 suggesting that it provides an appropriate low-level description of essential system properties.
88

89 ## Deciding between two options

90 Beginning with the simplest case, we consider the feedback between motion and internal
91 vectorial-computation when an animal is presented with two equally-attractive, but spatially-
92 discrete, options. In this case the activity of neurons encoding option 1, N_1 will be equal to
93 those encoding option 2, N_2 (Fig. 1A). Our model predicts that an animal moving, from a
94 relatively distant location, towards the two targets, will spontaneously compute the average
95 directional preference, resulting in corresponding motion in a direction oriented between the
96 two targets. As it approaches the targets, however, upon reaching a certain angular difference
97 between the options, the internal network undergoes a sudden transition in which it
98 spontaneously selects one, or the other, target (Fig. 1C). This results in an abrupt change in
99 trajectory, the animal being redirected towards the respective ‘selected’ target (Fig. 1C; see
100 also Fig. S3A for the same phenomenon occurring for a wide range of starting positions).
101

Our model therefore predicts that despite the fact that the egocentric geometrical relationship between the animal and the targets changes continuously, upon approaching the targets, there exists a location whereby a further, very small, increase in angular difference between the targets will result in a sudden change in system (neural) dynamics, and consequently in motion, and thus decision-making.

In numerical analysis of our model we find that irrespective of starting position, as the animal reaches the respective angle in space it will relatively suddenly select one of the options (Fig. S3A). While the specific angular difference at which this phenomenon occurs is dependent on neural tuning, ν (Fig. S3C), and the starting configuration (due to an interplay between the two timescales involved—for movement and for neural consensus, see Fig. S3B), it is always present as long as the neural noise, T remains below a critical firing rate, T_c (although even for $T < T_c$, these bifurcations may be difficult to see for small values of ν due to inherent noise in real biological systems; see Fig. S4 for simulations where vectorial representations of targets include directional error).

To gain a deeper insight into the mechanism underlying the observed spatiotemporal dynamics, we constructed a mean-field approximation (see SI Appendix) since this has the advantage of allowing us to conduct formal analyses of patterns realized in the simulated trajectories.

Geometric principles of decision-making

The mean-field analysis of our model shows that below a critical level of neural noise, animals will adopt the average among options as they approach the targets, until a critical phase transition upon which the system spontaneously switches to deciding among the options (Figs.

1B and S5A). Thus despite varying in its exact location (Fig. 1B), the sudden transition observed is an inevitable consequence of the system dynamics and will always occur.

Such sudden transitions correspond to 'bifurcations' in the mathematical study of dynamical systems. A bifurcation is said to occur when a smooth change in an external parameter, in this case perceived angular difference between the options, causes a sudden qualitative change in the system's behavior, here corresponding to a literal bifurcation (or branching) in physical space.

When dynamical systems undergo such a phase transition they exhibit a remarkable universal property: close to the phase transition, at the "critical-point" or "tipping-point", the system spontaneously becomes extremely sensitive to very small perturbations (e.g. to small differences in preference between options (16, 17)). This is true of both physical (e.g. magnetic (18)) and biotic systems (e.g. ecosystems (16, 19–21)) undergoing a phase transition. Correspondingly, we find that below a critical level of neural noise, the mean-field model exhibits a sudden increase in susceptibility as the animal approaches the critical point, immediately prior to the decision being made (Fig. S5A). Thus, as animals approach targets we predict they will pass through a window of space (corresponding to the critical angle for the respective geometry they are experiencing) in which their brain spontaneously becomes capable of discriminating between very small differences between options (e.g. a very small difference in neuronal activity being in 'favor' of one option; see Fig. S3D and SI Appendix for details). This highly-valuable property (for decision-making) is not built into the model, but is rather an emergent property of the inherent collective dynamics.

In many real biological systems, including the ones we consider here, the (neural) system size is typically not large enough to consider true phase transitions (which only occur for very large systems, as per the mean-field approximation), but rather 'phase-transition-like' behavior. Even though real biological systems are not necessarily close to the infinite size limit of the mean-field approximation, we see very similar dynamics for both small and large system sizes (Fig. S6).

Decision-making beyond two options

While the majority of decision-making studies consider only two options (due to both theoretical and experimental tractability (14, 22, 23)), animals moving in real space frequently encounter a greater number than this. Here we consider how animals will be expected to select among three, or more, options (possible targets) in space. First we begin with three identical options ($N_1 = N_2 = N_3$) since this gives us the clearest insight into the relationship between motion and decision-making dynamics. Then we relax these assumptions and consider differences between options (Fig. S3E) as well as a greater number of options (Fig. 2). Note that we do not modify our model in any way prior to introducing these additional complexities.

Below T_c (see SI Appendix and Fig. S7 for considerations when $T > T_c$), we once again find that the direction in which the animal moves is a function of the angular difference between the targets. When relatively far from the targets, it moves in the average of these three directions. Upon reaching a critical angular threshold between the leftmost and rightmost option (from the animal's perspective), however, the neural system spontaneously eliminates one of them and the animal begins moving in the direction average between the two remaining options (Fig. 1D and E). It continues in this direction until a second critical angle is reached, and now the animal eliminates one of the two remaining options and moves towards the only

175 remaining target (Figs. 1F and S5B). Thus we predict that the brain repeatedly breaks multi-
176 choice decisions into a series of binary decisions in space-time. Simulating a larger number of
177 options (Fig. 2) and varying environmental geometries (Figs. S8 and S9) demonstrates the
178 robustness of this mechanism in the face of environmental complexity and the more complex
179 spatial dynamics that emerge as organisms undergo repeated bifurcations.
180

181 ## Experimental tests of our predictions

182 Since the decision-process is sequential and depends on the geometry with respect to the targets
183 from an egocentric perspective, it can be visualized in the animals' trajectories. Our theoretical
184 studies make a key testable prediction: if neural groups within the decision-making ensemble
185 exhibit relatively local excitation, and long-range/global inhibition, we should observe
186 bifurcations in the animals' trajectories as they choose among identical options; and that if
187 animals face three (or more) such options, then the complex decision task should be broken
188 down to a series of binary decisions.
189

190 Since the geometrical principles revealed above are expected to be both robust and generic, we
191 use immersive virtual reality (24) (Fig. S10) to test our predictions by investigating both two-
192 and three-choice decision-making in three evolutionarily highly-divergent brains under
193 ecologically-relevant scenarios: fruit flies (*Drosophila melanogaster*) and desert locusts
194 (*Schistocerca gregaria*) deciding which among multiple vertical objects to approach (e.g. to
195 perch), and zebrafish (*Danio rerio*) choosing with which conspecific(s) to school.
196 Like many other insects (25–28), fruit flies (29) and desert locusts (30) exhibit a natural
197 tendency to orient and move towards high-contrast vertical features (potential landing sites or
198 indicators of vegetation) in their environment. We exploit this tendency, presenting multiple
199 identical black pillars as targets in an otherwise white environment. We record trajectories of

our focal animals (solitary flies or locusts) as they choose to move towards one of these pillars, thus obtaining a behavioral readout of the decision-making process (see SI Appendix for experimental details; Figs. S11 and S12 show raw trajectories of flies and locusts respectively).

As predicted by our theory (Fig. 1B and C), we find that, in the two-choice case, both flies and locusts initially move in the average of the egocentric target directions until a critical angular difference, at which point they select (randomly) one, or the other, option and move towards it (randomization test where $y-$coordinates between trajectories were swapped showed that the bifurcation fit to our experimental data was highly significant; $p < 0.01$ for both flies and locusts; Fig. 1G). In the three-choice case, the animals' movements are also consistent with our theory; as predicted (Fig. 1E and F) they break the three-choice decision into two sequential binary decisions ($p < 10^{-4}$ for both flies and locusts; Fig. 1H). For both animals, the observed angle of bifurcation ($\sim 110^{o}$ for flies and $\sim 90^{o}$ for locusts) is much larger than their visual spatial resolution ($\sim 8^{o}$ and $\sim 2^{o}$ for flies (31) and locusts (32, 33).

Our zebrafish experiments consider spatial decision-making in a social context. We present virtual conspecifics (see SI Appendix for methodological details) that move back-and-forth in the arena parallel to each other as targets (Figs. 3A and S13A) and behave (Fig. S14), and are responded to (Fig. S15), in the same way as real fish. Because they are social, the real fish respond to these virtual fish by tending to follow at a (relatively) fixed distance behind them (Fig. S13E). Our data are best represented within this moving frame of reference (the virtual fish; Fig. S13). Theoretically we predict that for two virtual fish we should see a single bifurcation, where the real fish will suddenly switch from averaging the target directions to deciding among them (i.e. swimming predominantly with one of the virtual fish), as a function of increasing the lateral distance, L, between the virtual fish (Figs. 3B and S16; see SI Appendix

for details of model implementation). The existence of this bifurcation is clearly seen in our experiments (Fig. 3C). When considering three moving virtual conspecifics, the model predicts that real fish will spontaneously break the three-choice decision to two binary decisions, and a comparison of the theoretical prediction and experimental results demonstrates this to be the case (c.f. Fig. 3E and F). Although detailed models considering the specifics of each system would be expected to provide additional quantitative fits (at the expense of losing some degree of generality and analytical tractability), our results are broadly independent of the model implementation details. Thus, we find that the key predictions of our model are validated in fruit flies, desert locusts and larval zebrafish in distinct, yet ecologically relevant contexts.

Our results demonstrate that, across taxa and contexts, explicitly considering the time-varying geometry during spatial decision-making provides new insights that are essential in order to understand how, and why, animals move the way they do. The features we have revealed are highly robust, and we predict that they occur in decision-making processes across various scales of biological organisation, from mobile neural groups (individuals) to animal collectives (see Supplementary Fig. 17, Supplementary Fig. 18 and Supplementary Information), suggesting they are general features of spatiotemporal computation. In addition, while here we investigate relatively simple decisions allowing us to reveal the geometrical principles at work, this framework—and the fundamental features outlined here—can readily serve as a general foundation for future investigations of more complex aspects of spatial decision-making.

A link to collective decision-making

In the two-choice context, our results of individual decision-making are reminiscent of collective decision-making in animal groups (fish schools (34), bird flocks (35) and baboon troops (22)). In order to draw a formal link between these two scales of biological

organization—decision-making in the brain, and decision-making in animal groups—we consider a model of collective decision-making (36) with equal number of individuals exhibiting preference for each target (see SI Appendix for methodological details). Consistent with our above results, we find that even in groups, animals must reduce multi-choice decisions to a series of binary decisions (Fig. 4). Thus, our work provides a first evidence that similar principles underlie decision-making in distinct systems across multiple scales of biological organization. Furthermore, by presenting social interactions in a decision-making context, our zebrafish experiments elucidate the neural basis of schooling allowing us to glean insights across three scales of biological organization—from neural dynamics to individual decisions, and from individual decisions to collective movement.

Conclusions

We demonstrate that, across taxa and contexts, explicitly considering the time-varying geometry during spatial decision-making provides new insights that are essential to understand how, and why, animals move the way they do. The features revealed here are highly robust, and we predict that they occur in decision-making processes across various scales of biological organization, from individuals to animal collectives (see Figs. 4 and S18, and SI Appendix), suggesting they are fundamental features of spatiotemporal computation.

References

1. C. E. J. Kennedy, J. A. Endler, S. L. Poynton, H. McMinn, Parasite load predicts mate choice in guppies. *Behav Ecol Sociobiol* **21**, 291–295 (1987).

2. K. Summers, R. Symula, M. Clough, T. Cronin, Visual mate choice in poison frogs. *Proceedings of the Royal Society of London. Series B: Biological Sciences* **266**, 2141–2145 (1999).

3. E. Forsgren, Predation Risk Affects Mate Choice in a Gobiid Fish. *The American Naturalist* **140**, 1041–1049 (1992).

4. R. Kiani, L. Corthell, M. N. Shadlen, Choice Certainty Is Informed by Both Evidence and Decision Time. *Neuron* **84**, 1329–1342 (2014).

5. J. M. Beck, *et al.*, Probabilistic Population Codes for Bayesian Decision Making. *Neuron* **60**, 1142–1152 (2008).

6. A. K. Churchland, R. Kiani, M. N. Shadlen, Decision-making with multiple alternatives. *Nature Neuroscience* **11**, 693–702 (2008).

7. S. S. Kim, H. Rouault, S. Druckmann, V. Jayaraman, Ring attractor dynamics in the Drosophila central brain. *Science* **356**, 849–853 (2017).

8. J. D. Seelig, V. Jayaraman, Neural dynamics for landmark orientation and angular path integration. *Nature* **521**, 186–191 (2015).

9. J. S. Taube, R. U. Muller, J. B. Ranck, Head-direction cells recorded from the postsubiculum in freely moving rats. II. Effects of environmental manipulations. *Journal of Neuroscience* **10**, 436–447 (1990).

10. A. Finkelstein, *et al.*, Three-dimensional head-direction coding in the bat brain. *Nature* **517**, 159–164 (2015).

11. A. Sarel, A. Finkelstein, L. Las, N. Ulanovsky, Vectorial representation of spatial goals in the hippocampus of bats. *Science* **355**, 176–180 (2017).

12. Ø. A. Høydal, E. R. Skytøen, S. O. Andersson, M.-B. Moser, E. I. Moser, Object-vector coding in the medial entorhinal cortex. *Nature* **568**, 400–404 (2019).

13. R. Wehner, B. Michel, P. Antonsen, Visual navigation in insects: coupling of egocentric and geocentric information. *Journal of Experimental Biology* **199**, 129–140 (1996).

14. A. Bahl, F. Engert, Neural circuits for evidence accumulation and decision making in larval zebrafish. *Nature Neuroscience* **23**, 94–102 (2020).

15. I. Pinkoviezky, I. D. Couzin, N. S. Gov, Collective conflict resolution in groups on the move. *Physical Review E* **97** (2018).

16. L. Benedetti-Cecchi, L. Tamburello, E. Maggi, F. Bulleri, Experimental perturbations modify the performance of early warning indicators of regime shift. *Current Biology* **25**, 1867–1872 (2015).

17. A. Gelblum, *et al.*, Ant groups optimally amplify the effect of transiently informed individuals. *Nature Communications* **6** (2015).

18. B. M. McCoy, T. T. Wu, *The two-dimensional Ising model: second edition* (Courier Corporation, 2014).

19. C. Boettiger, A. Hastings, From patterns to predictions. *Nature* **493**, 157–158 (2013).

20. C. Wissel, A universal law of the characteristic return time near thresholds. *Oecologia* **65**, 101–107 (1984).

21. T. M. Lenton, Early warning of climate tipping points. *Nature Climate Change* **1**, 201–209 (2011).

22. A. Strandburg-Peshkin, D. R. Farine, I. D. Couzin, M. C. Crofoot, Shared decision-making drives collective movement in wild baboons. *Science* **348**, 1358–1361 (2015).

23. R. Ratcliff, P. L. Smith, S. D. Brown, G. McKoon, Diffusion Decision Model: Current Issues and History. *Trends in Cognitive Sciences* **20**, 260–281 (2016).

24. J. R. Stowers, *et al.*, Virtual reality for freely moving animals. *Nature Methods* **14**, 995–1002 (2017).

25. T. Poggio, W. Reichardt, A theory of the pattern induced flight orientation of the fly Musca domestica. *Kybernetik* **12**, 185–203 (1973).

26. D. Varju, Stationary and dynamic responses during visual edge fixation by walking insects. *Nature* **255**, 330–332 (1975).

27. W. Reichardt, T. Poggio, A theory of the pattern induced flight orientation of the fly Musca domestica II. *Biological Cybernetics* **18**, 69–80 (1975).

28. P. K. Kaushik, M. Renz, S. B. Olsson, Characterizing long-range search behavior in Diptera using complex 3D virtual environments. *PNAS* **117**, 12201–12207 (2020).

29. E. Horn, R. Wehner, The mechanism of visual pattern fixation in the walking fly, Drosophila melanogaster. *Journal of Comparative Physiology A* **101**, 39–56 (1975).

30. G. K. Wallace, Some experiments on form perception in the nymphs of the desert locust, Schistocerca gregaria forskål. *Journal of Experimental Biology* **35**, 765–775 (1958).

31. P. T. Gonzalez-Bellido, T. J. Wardill, M. Juusola, Compound eyes and retinal information processing in miniature dipteran species match their specific ecological demands. *Proceedings of the National Academy of Sciences* **108**, 4224–4229 (2011).

32. O. Faivre, M. Juusola, Visual coding in locust photoreceptors. *Plos One* **3**, e2173 (2008).

33. M. Wilson, Angular sensitivity of light and dark adapted locust retinula cells. *Journal of Comparative Physiology* **97**, 323–328 (1975).

34. I. D. Couzin, *et al.*, Uninformed individuals promote democratic consensus in animal groups. *Science* **334**, 1578–1580 (2011).

35. D. Biro, D. J. T. Sumpter, J. Meade, T. Guilford, From compromise to leadership in pigeon homing. *Current Biology* **16**, 2123–2128 (2006).

36. I. D. Couzin, J. Krause, N. R. Franks, S. A. Levin, Effective leadership and decision-making in animal groups on the move. *Nature* **433**, 4 (2005).

Materials and Methods

We construct a simple, spatially-explicit model of neural decision-making to study how the brain reduces choice in the presence of numerous spatial options (adapted from (15)). Theoretical predictions obtained were then tested experimentally by exposing invertebrate (fruit flies and desert locusts) and vertebrate systems (zebrafish) to spatial choice tests in virtual reality. To identify unifying principles of spatiotemporal computation across scales of biological organisation, we also reproduce the obtained decision-making patterns with an established model of collective decision-making in animal groups.

Neural decision-making model. We construct a simple, spatially-explicit model of neural decision-making that takes directions to different options (potential 'targets' in space) as input, and outputs a vectorial representation ('activity bump') of its desired direction of motion (15). Here, the animal's brain is characterized by a neural network composed of N neurons. Each neuron i encodes direction to one of the presented goals $\hat{p}_i$, and exists in one of two states: $\sigma_i = 0$ ("not firing") or $\sigma_i = 1$ ("firing"). The energy of the system (for any given configuration) is given by its Hamiltonian, H.

$$H = -\frac{k}{N}\sum_{i \neq j} J_{ij}\sigma_i\sigma_j$$

where, k is the number of options available to the individual and J_{ij} is the interaction strength between neurons i and j. Here, J_{ij} is given by

$$J_{ij} = \cos\left(\pi\left(\frac{|\theta_{ij}|}{\pi}\right)^{\nu}\right)$$

where, θ_{ij} is the angle between preferred directions of neurons i and j, and ν represents the neural tuning parameter. For $\nu = 1$, the interactions become "cosine-shaped" $J_{ij} = \cos(\theta_{ij})$, and the network has a Euclidean representation of space (Fig. S1). For $\nu < 1$, the network has more local excitation and encodes space in a non-Euclidean manner (Fig. S1). System

dynamics are implemented by energy minimization using the Metropolis-Hastings algorithm (similar to other Ising spin models) and the agent then moves with a velocity $\vec{V}$ determined by the normalized sum of goal vectors $\hat{p}_i$ of all active neurons.

$$\vec{V} = \frac{v_0}{N} \sum_{i=1}^{N} \hat{p}_i \, \sigma_i$$

where v_0 is the proportionality constant. The goal vector $\hat{p}_i$ now points from the agent's updated location to the neuron's preferred goal with directional noise chosen from a circularly wrapped Gaussian distribution centered at 0 with a standard deviation σ_e. As in the mean-field approximation of the model, the timescale of movement (defined by the typical time to reach the target) in the numerical simulations was set to be much greater than the timescale of neural firing (the typical time between two consecutive changes in the neural states σ_i).

Collective decision-making model. We reproduce results from our neural decision-making model in a model that describes spatial decision-making at a different scale of biological organization (refer (36) for methodological details). To highlight the features that are key to producing the observed bifurcation patterns, we run simulations with and without feedback on the strength of goal-orientedness of individuals.

Fly virtual reality experiments. All experiments were conducted on 3- to 5-day old female wild-type CS strain *Drosophila melanogaster* raised at 26℃ on a 12 hr light, 12 hr dark cycle. Experiments were conducted in a flyVR setup procured from loopbio GmbH. 60 tethered *Drosophila melanogaster* were exposed to either a two-choice or a three-choice decision task (30 and 30 individuals, respectively) in the virtual reality environment. Each experimental trial lasted 15 min where flies were exposed to five sets of stimuli—three experimental sets and two control sets. The experimental stimuli sets consisted of two or three black cylinders (depending

393 on the experimental condition) that were presented to the animal in an otherwise white
394 environment. A control stimulus with a single pillar was presented before and after the
395 experimental conditions. We rotated all trajectories such that the $x-$axis points from the
396 origin, to the centre of mass of the targets. To visualise trajectories in the various experimental
397 conditions, we created time-normalised (proportion of maximum across a sliding time window)
398 density maps. We then folded the data about the line of symmetry, $y = 0$ and applied a density
399 threshold to the time-normalised density map. A piecewise phase transition function was then
400 fit to quantify the bifurcation.

401 $$y = \begin{cases} 0 & x \leq x_c \\ A|x - x_c|^{\alpha} & x > x_c \end{cases}$$

402 where x_c is the critical point, α is the critical exponent, and A is the proportionality constant.
403 We also performed randomisation tests for each bifurcation where we conducted the exact fit
404 procedure described above to data where the trajectories were randomised by keeping the x-
405 coordinates, and swapping the y-coordinates with values from other random events.
406 Randomizations show that the resultant fit to our experimental data were highly significant
407 ($p < 0.01$ for binary choice and $p < 10^{-4}$ for the three-choice case).
408
409 **Locust virtual reality experiments.** All experiments were conducted on 156 instar 5 desert
410 locusts (57 individuals for two-choice and 99 individuals for three-choice experiments,
411 respectively) raised in the Animal Research Facility of the University of Konstanz.
412 Experiments were conducted in a locustVR setup procured from loopbio GmbH. The
413 experimental procedure was identical to the one described above for flies, except now, each
414 experimental trial lasted 48 min—three experimental sets (12 min each) and two control sets
415 (6 min each). Analysing bifurcations in locust trajectories using the same methods described
416 above showed that the resultant bifurcations fit to our experimental data were highly significant
417 ($p < 0.01$ for binary choice and $p < 10^{-4}$ for the three-choice case).

Fish virtual reality experiments. All experiments were conducted on 1 cm $\pm$ 0.1 cm long zebrafish of age 24 to 26 days post-fertilisation raised in a room at 28℃ on a 16 hr light, 8 hr dark cycle. 390 fish were tested in total. Of these, 198 fish were exposed to decision-making with two virtual targets, and 39 fish exposed to decision-making with three virtual targets (see Supplementary Information for more details). Experiments were conducted in a fishVR setup procured from loopbio GmbH (refer (24) for details). Once a fish was introduced in the arena, it was given 20 min to acclimatise to the environment. This was followed by a 10 min control where it was presented a single virtual conspecific circling the arena in a circle of radius 8 cm. After this, the real fish was exposed to choice experiments that lasted 90 min with the virtual fish initialised with random lateral distances between them and random swim direction. To visualise the bifurcations, we normalised (proportion of maximum) and stacked the marginal distributions along the direction of the virtual fish's motion for various lateral distances. All experiments were conducted in accordance with the animal ethics permit approved by Regierungspräsidium Freiburg, G-17/170.

Acknowledgements. We thank all members of the Department of Collective Behaviour who assisted with the project: Renaud Bastien for discussions and help setting up the VR experiments, Guy Amichay for providing control data of two real fish swimming together, and Paul Szyszka for showing V.H.S. how to tether flies. We thank the 'Itai Cohen Lab' for the fruit fly image used in Fig. \ref{fig:insects} and Andreas Poehlmann, John Stowers and Max Hofbauer from loopbio GmbH for technical support with the VR systems. V.H.S., L.L., B.R.S. and I.D.C. are also grateful to the animal care at the University of Konstanz including Christine Bauer, Jayme Weglarski and Dominique Leo for help in conducting the experiments. They also acknowledge the efforts of the scientific and technical staff at the University of Konstanz

including Michael Mende, Markus Miller, Mäggi Hieber Ruiz and Daniel Piechowski. V.H.S. acknowledges the International Max Planck Research School (IMPRS) for Organismal Biology for the graduate school community and access to courses and resources. I.D.C. acknowledges support from the NSF (IOS-1355061), the Office of Naval Research grant (ONR, N00014-19-1-2556), the Struktur- und Innovationsfonds für die Forschung of the State of Baden-Württemberg, the Deutsche Forschungsgemeinschaft (DFG, German Research Foundation) under Germany's Excellence Strategy-EXC 2117-422037984 and the Max Planck Society. N.S.G. is the incumbent of the Lee and William Abramowitz Professorial Chair of Biophysics and acknowledges support by the Minerva Foundation (grant no. 712601). M.N acknowledges support from the Hungarian Academy of Sciences (a grant to the MTA-ELTE 'Lendület' Collective Behaviour Research Group, grant number 95152, and MTA-ELTE Statistical and Biological Research Group) and Eötvös Loránd University.

Author contributions. V.H.S. and I.D.C. designed the study; V.H.S., D.G., T.S., N.S.G. and I.D.C. constructed the model; D.G. and N.S.G. constructed the mean-field approximation; V.H.S. and I.D.C. designed the fly experiments; V.H.S. conducted these experiments and analyzed the data with L.L. and M.N.; V.H.S., B.R.S. and I.D.C. designed the locust experiments; B.R.S. conducted these experiments and V.H.S. analyzed the data with M.N.; L.L. and I.D.C. designed the fish experiments; L.L. conducted these experiments and analyzed this data with V.H.S. and M.N.; V.H.S. and I.D.C. drafted the manuscript with significant contributions from all authors.

Competing interests. The authors declare that they have no competing interests.

Figures.

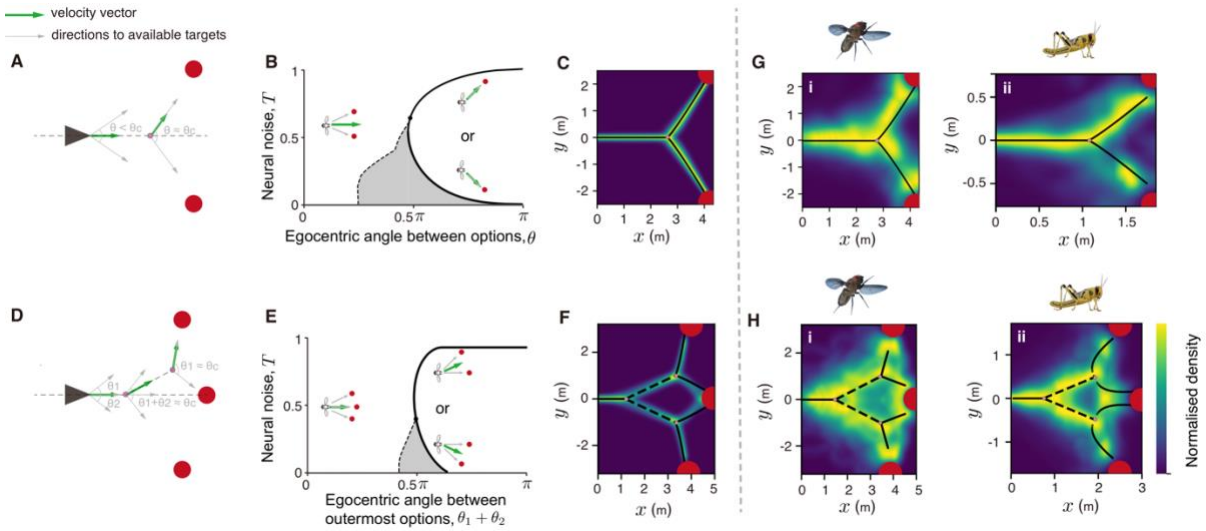

Fig. 1. Geometrical principles of two-choice and three-choice decision-making. (A) Schematic of the binary decision-making experiments. This simplified representation shows that a sharp transition in the animal's direction of travel is expected near a critical angle, θ_c. (B) A phase diagram describing the 'critical' transition exhibited while moving from compromise to decision between two options in space. The shaded area (also in E) represents the region in parameter space where both the compromise, and the decision solutions exist. (C) Density plot showing trajectories predicted by the neural model in a two-choice context. The axes represent $x-$ and $\$y-$coordinates in Euclidean space. The black line (also in G) presents a piecewise phase-transition function fit to the bifurcation. (D) Schematic of three-choice decision-making experiments, where the central target is on the angle bisector of the angle subtended by the other two targets. (E) A phase diagram describing the first 'critical' transition when the individual chooses among three options. Once the individual eliminates one of the outermost targets, it can decide between the two remaining options, similar to the two-choice phase diagram described in B. (F) Theoretical predictions for decision-making in a three-choice context. The dashed line (also in H) is the bisector of the angle subtended by center target and the corresponding side target on the first bifurcation point. See Table S1 for parameters used

484 in C and F. (G) and (H) Density plots from experiments conducted with flies and locusts

485 choosing among two and three options, respectively.

486

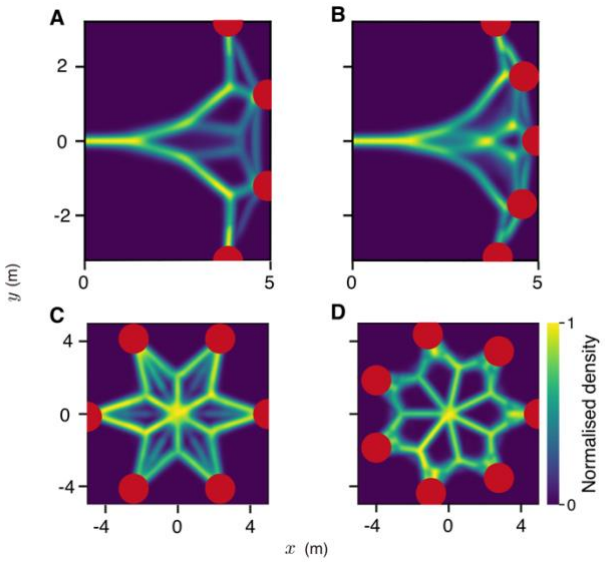

Fig. 2. Decision-making for a larger number of targets. Density plots of simulated trajectories for four- (A), five- (B), six- (C) and seven-choice (D) decision-making when targets are placed equidistant and equiangular from the agent. Thee axes represent $x-$ and $y-$coordinates in Euclidean space. Geometrical configurations are also varied to place the targets on the same side of the agent (A and B) or in radial symmetry (C and D). See Table S1 for parameters used in A–C. In D, all parameters used are identical except the system size $N = 70$.

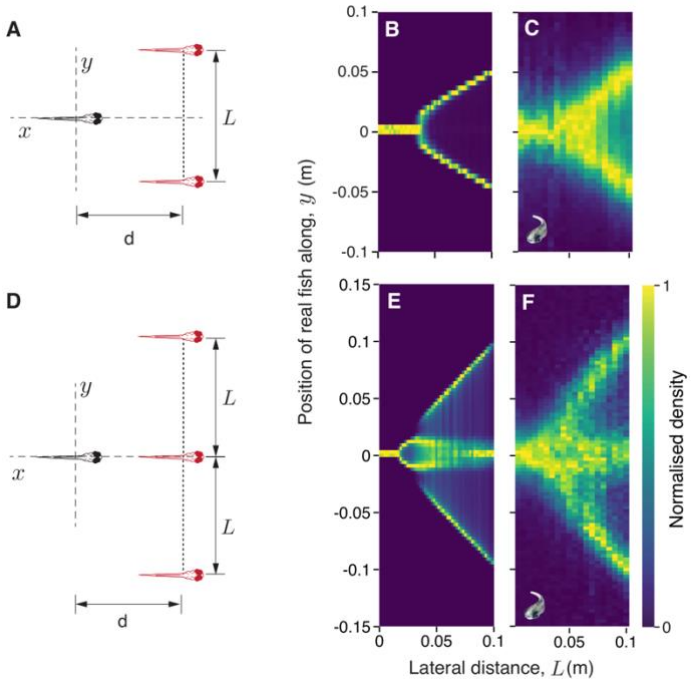

Fig. 3. Decision-making in a moving frame-of-reference. (A) Schematic of the two-choice decision-making experiments conducted with larval zebrafish. In these experiments (also in the three-choice experiments depicted in D), the virtual fish swim parallel to each other while maintaining a fixed lateral distance, *L* between them. We only consider data where the real fish swims behind the virtual fish, i.e., it follows the virtual fish (see SI Appendix and Fig. S13 for details). (B) Normalized probability distribution (proportion of maximum) of simulated positions of an agent following two moving targets, and corresponding experiments (C) conducted with larval zebrafish following two virtual conspecifics. (D) Schematic representation of the three-choice decision-making experiments. (E) Normalized probability distributions of simulated positions of an agent following three moving targets, and corresponding experiments (F) conducted with larval zebrafish following three virtual conspecifics. See Table S1 for model parameters used in B and E.

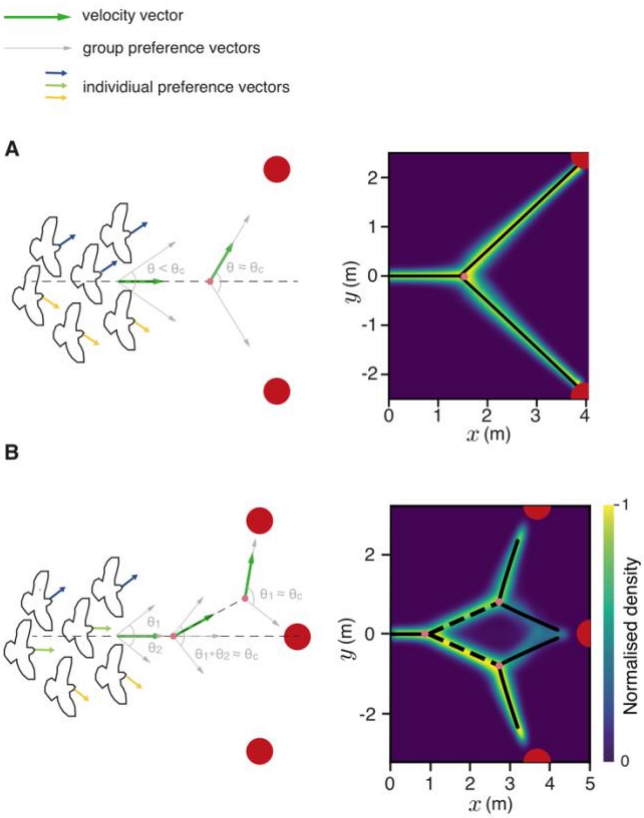

Fig. 4. Consensus decision-making in simulations of animal groups follow the same geometrical principles. Results for two- (A) and three-choice (B) decision-making in a model of animal collectives. The density plots show trajectories adopted by the centroid of the animal group for 500 replicate simulations where the groups don't split. The axes represent $x-$ and $y-$coordinates in Euclidean space. The black lines show a piecewise phase-transition function fit to the trajectories. For the three-choice case (B), the dashed line is the bisector of the angle subtended by center target and the corresponding side target on the first bifurcation point. See Table S2 for parameters used.